A Photovoltaic Solar Pump with Microprocessor Control and One-Axis Tracking

Part I: The solar resource and the design of the low concentration PV system.

Part II: Design of the microcomputer control system.

C.L. Teoh, D.G.S. Chuah, S.L. Lee and G.S. Rao
School of Physics & School of Mathematics
Universiti Sains Malaysia, 11800 USM Penang, Malaysia

ABSTRACT

A study of a low-concentration photovoltaic (PV) water pumping system with a microprocessor control and battery back-up subsystem is presented. The design of the system is based on the statistical results of the solar radiation in Penang, Malaysia from 1975 to 1980 and on a forecast solar radiation of two times concentration using plane mirrors, the PV module characteristics, the effect of series resistance and the temperature's effect on the efficiency of the system. Further improvements in the efficiency of the water pumping system are obtained with the design of a microprocessor-based control subsystem to manage the energy sources and an one-axis tracking system.

INTRODUCTION

A study of a 100-watt A.C. water pumping system using a microprocessor and a battery back-up system is presented. The design of the system is based on the statistical results of solar radiation in Penang from 1975 to 1980. A forecast solar radiation of two times concentration using mirrors is used to construct the photovoltaic array after taking into consideration the effect of series resistance and temperature and the temperature's effect on the efficiency of the system. The efficiency of the water pumping system is improved further with the design of a microprocessor-based control subsystem to manage the energy sources (solar and battery) and a one-axis tracking system.

The study is divided basically into three parts, namely (I) the solar resource and the design of the low concentration PV system, (II) design of the microcomputer control system and (III) the performance data and analysis of the microcomputer PV system. Parts I and II are discussed in this issue with Part III to follow in the next issue.

PART I: THE SOLAR RESOURCE AND THE DESIGN OF THE LOW CONCENTRATION PV SYSTEM

Forecasting Performance Based on Solar Radiation

Data for Penang (1975-1980)

The histograms for the mean hourly global radiation and direct radiation data for Penang from 1975-1980 were smoothed out using spline functions.[1] Based on the smoothed values and the concentration factor of two (to be discussed in the following paragraph), the forecast performance of the system can be obtained as follows:

A low concentrator using booster mirrors receives both diffuse and direct solar radiation.

Assuming that the concentration factor of two only applies to direct radiation, the total solar radiation falling on the horizontal PV module after concentration is:

$$Q = D + 2I_d \tag{1}$$

where Q = sum of total of solar radiation after concentration

D = diffuse solar radiation

I_d = direct solar radiation on the horizontal surface.

But the global solar radiation (I_g), diffuse (D) and direct beam radiation (I_o) are related by the following usual equation:

$$I_g = D + I_o \sin\theta = D + I_d \tag{2}$$

where θ is the solar altitude.

Substituting (2) in (1), gives

$$Q = I_g + I_d \tag{3}$$

Thus, the total radiation falling on the solar module with a concentration factor of 2 can be obtained by merely adding the global solar radiation and the direct solar radiation on the horizontal surface. Based on (3), the forecast available hourly mean total radiation falling on the horizontal photovoltaic modules is plotted and shown in Figs. 1-12.

Construction of a low concentration PV electric generator

Firstly, a conventional photovoltaic module was characterized under a test-bed to obtain the optimum concentration factor of 2 under varying illumination levels and module temperatures.

The current-voltage characteristics of the module were obtained for intensity varying from 50 mW/cm^2 to 400 mW/cm^2 and at temperatures of 25°C, 45°C and 60°C. The resulting current-voltage (I-V) curves are shown in Figs. 13-15.

From these data, the maximum power ($P_{max} = V_{max}\ I_{max}$) and the curve factor (C.F.) = ($V_{max}\ I_{max}/V_{oc}\ I_{sc}$) were calculated, where P_{max}, V_{max}, I_{max} are the maximum power, voltage

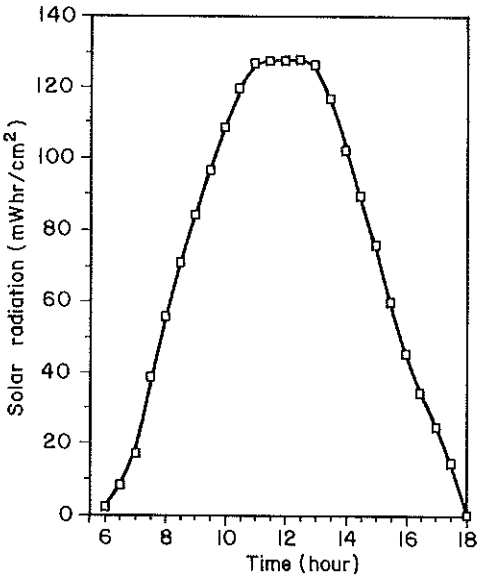

Fig. 1 Forecast 2X (two times) concentration solar radiation for January.

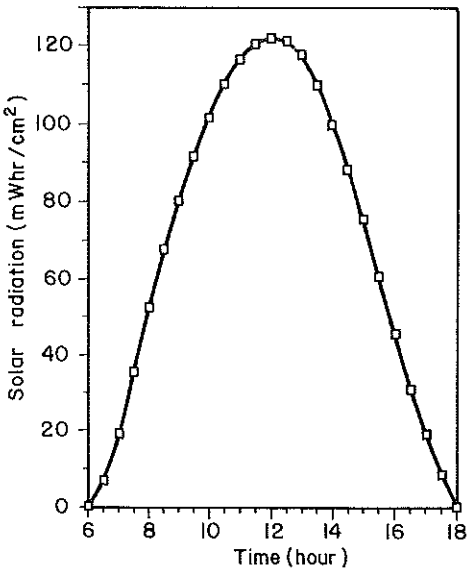

Fig. 2 Forecast 2X (two times) concentration solar radiation for February.

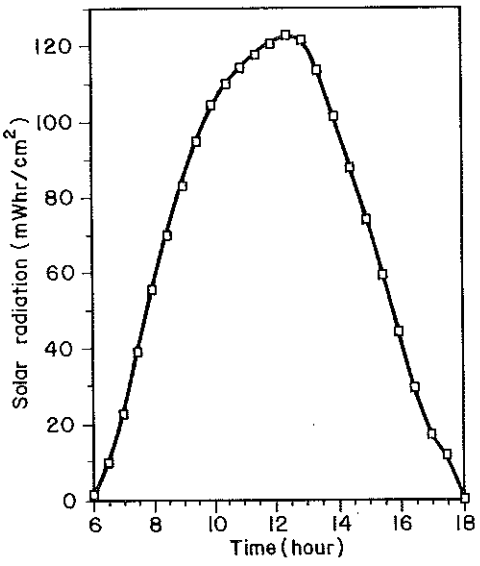

Fig. 3 Forecast 2X (two times) concentration solar radiation for March.

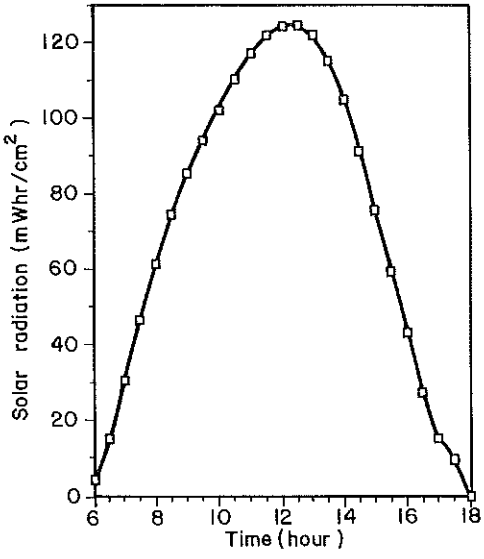

Fig. 4 Forecast 2X (two times) concentration solar radiation for April.

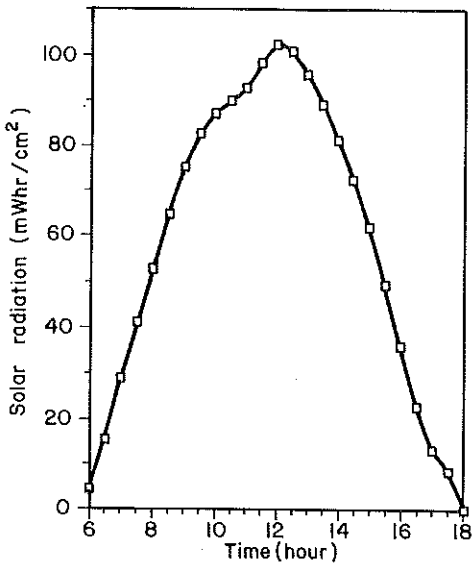

Fig. 5 Forecast 2X (two times) concentration solar radiation for May.

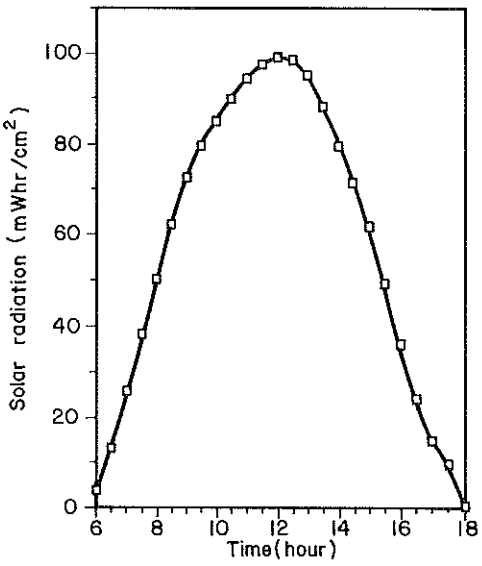

Fig. 6 Forecast 2X (two times) concentration solar radiation for June.

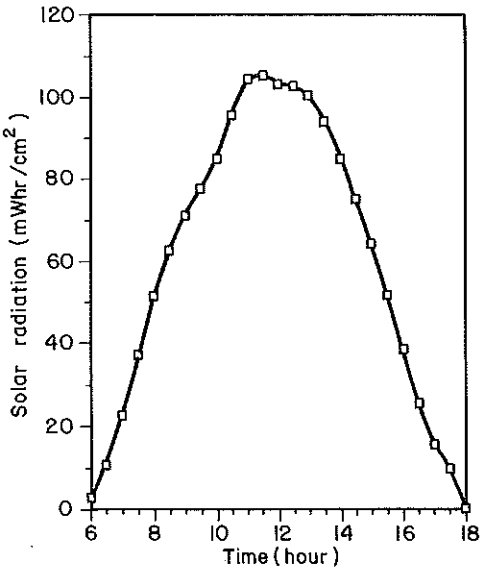

Fig. 7 Forecast 2X (two times) concentration solar radiation for July.

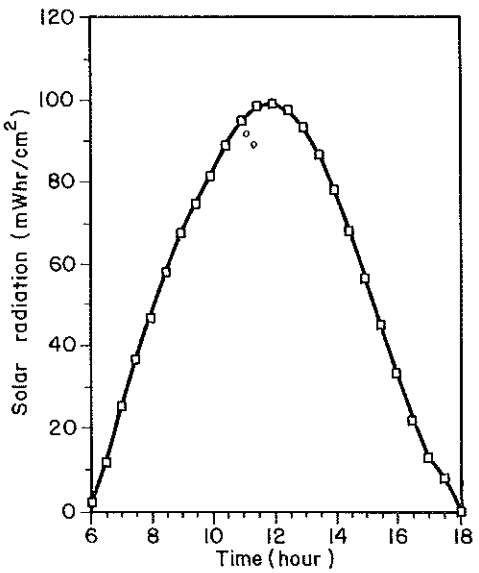

Fig. 8 Forecast 2X (two times) concentration solar radiation for August.

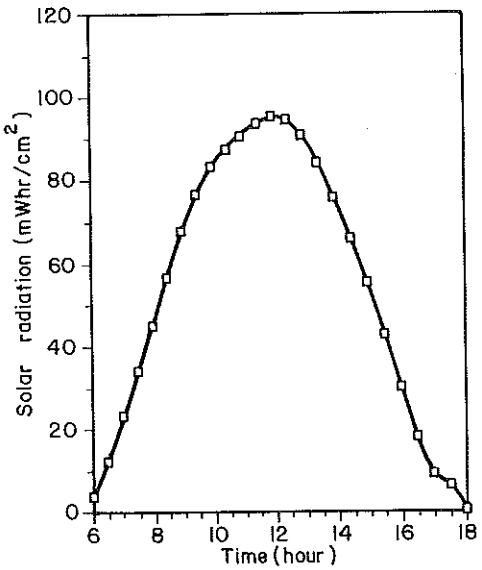

Fig. 9 Forecast 2X (two times) concentration solar radiation for September.

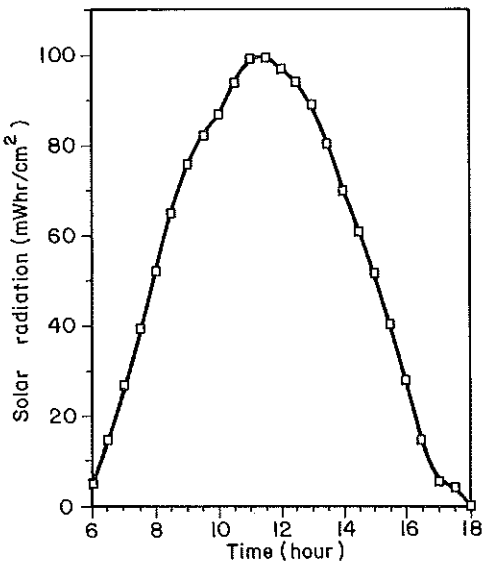

Fig. 10 Forecast 2X (two times) concentration solar radiation for October.

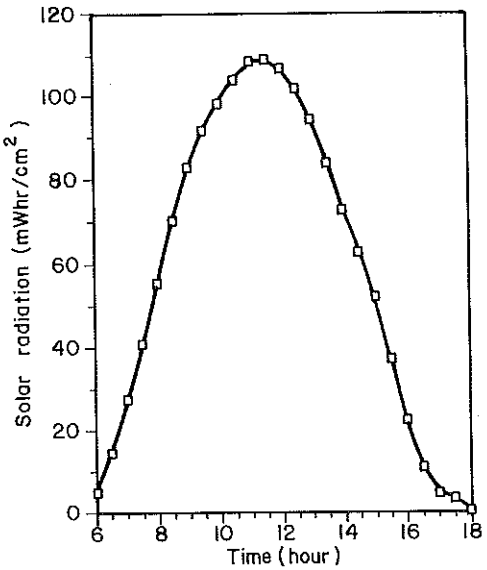

Fig. 11 Forecast 2X (two times) concentration solar radiation for November.

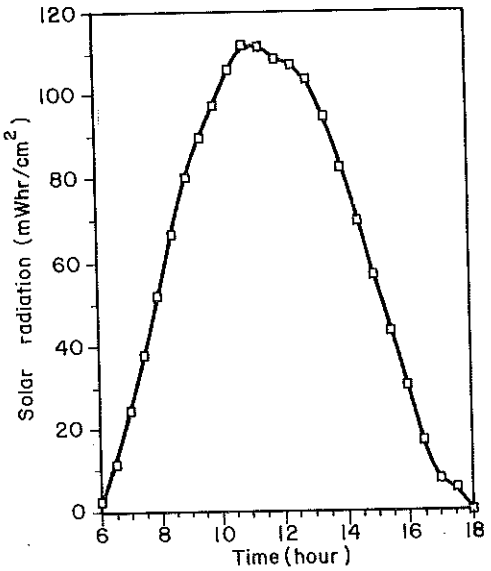

Fig. 12 Forecast 2X (two times) concentration solar radiation for December.

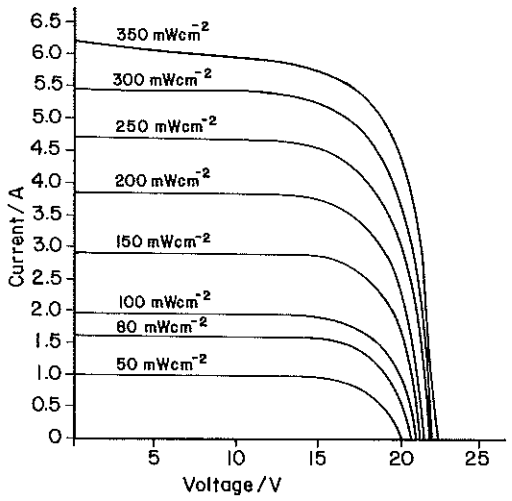

Fig. 13 Current-voltage characteristics (25°C).

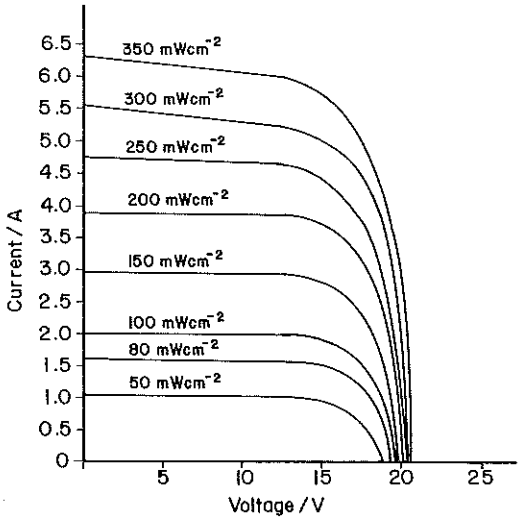

Fig. 14 Current-voltage characteristics (45°C).

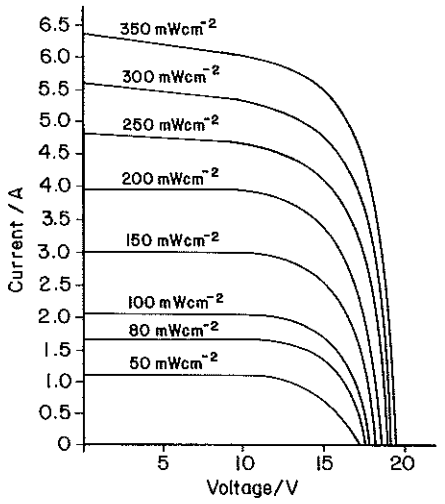

Fig. 15 Current-voltage characteristics (60°C).

and current respectively; V_{oc} and I_{sc} are the open circuit voltage and short circuit current respectively. The encapsulated cell efficiency was then obtained from

$$\eta_{ec} = \frac{\text{C.F. } V_{oc}\, I_{sc}}{P_I} \tag{4}$$

where P_I is the incident power as measured by the Solarex reference cell #073.

The overall module efficiencies were also calculated using the equation

$$\eta = \frac{\text{maximum power}}{\text{module area} \times \text{incident irradiance}} \quad (5)$$

The module efficiencies thus calculated include losses arising from electrical mismatch of the cells, I^2R losses in the cell interconnectors and module buses and leads, optical transmission losses, illumination mismatch and module packing efficiency. The module efficiencies are also tabulated in Table 1. Some values of the parameters given by the manufacturer are compared with the experimental values in Table 2. There is reasonably close agreement between the experimental and manufacturer's values, as indicated in Figs. 16-17[2].

Table 1
Measured data and calculated values of a conventional photovoltaic module

Temperature	Parameter	Values of the parameter for the following intensities							
		50 mW cm^{-2}	80 mW cm^{-2}	100 mW cm^{-2}	150 mW cm^{-2}	200 mW cm^{-2}	250 mW cm^{-2}	300 mW cm^{-2}	350 mW cm^{-2}
25°C	V_{oc} (V)	20.2	20.8	21.1	21.3	21.6	21.9	22.1	22.4
	I_{sc} (A)	1.00	1.60	1.95	2.90	3.85	4.70	5.45	6.20
	Maximum voltage (V)	16.5	16.8	16.9	17.3	17.5	17.75	18.1	18.5
	Maximum current (A)	0.90	1.50	1.83	2.65	3.45	4.18	4.75	5.20
	Maximum power (W)	14.85	25.20	30.93	45.85	60.38	74.10	85.98	96.20
	Curve factor	0.74	0.76	0.75	0.74	0.73	0.72	0.71	0.69
	Encapsulated cell efficiency	12.13	12.87	12.64	12.49	12.34	12.11	11.71	11.23
	Module efficiency	7.60	8.01	7.87	7.77	7.68	7.54	7.29	6.99
45°C	V_{oc}(V)	18.9	19.3	19.6	19.8	20.1	20.3	20.4	20.6
	I_{sc}(A)	1.05	1.60	2.00	2.95	3.90	4.75	5.55	6.30
	Maximum voltage (V)	15.5	15.7	15.9	16.1	16.4	16.6	16.8	17.1
	Maximum current (A)	0.93	1.50	1.85	2.70	3.53	4.13	4.73	5.29
	Maximum power (W)	14.42	23.55	29.42	43.47	57.81	68.48	79.38	89.93
	Curve factor	0.73	0.76	0.75	0.74	0.73	0.71	0.70	0.69
	Encapsulated cell efficiency	11.78	12.03	12.02	11.84	11.81	11.19	10.81	10.50
	Module efficiency	7.38	7.49	7.48	7.37	7.35	6.97	6.72	6.53
60°C	V_{oc}(V)	17.2	17.6	17.9	18.2	18.6	19.0	19.1	19.4
	I_{sc}(A)	1.10	1.65	2.05	3.00	3.95	4.80	5.60	6.35
	Maximum voltage (V)	13.8	13.9	14.0	14.3	14.8	15.3	15.8	16.0
	Maximum current (A)	0.90	1.50	1.85	2.68	3.45	4.05	4.60	5.23
	Maximum power (W)	12.42	20.85	25.90	38.32	51.06	61.97	72.68	84.13
	Curve factor	0.69	0.72	0.71	0.70	0.69	0.68	0.68	0.68
	Encapsulated cell efficiency	10.15	10.65	10.58	10.44	10.43	10.13	9.90	9.82
	Module efficiency	6.36	6.66	6.59	6.50	6.49	6.30	6.16	6.11

Note: The above table is extracted from p. 225 of *Solar Cells*, Vol. 10 (1983), Teoh et al.[2]

Table 2
Comparison of experimental values of the parameters with those given by the manufacturer

Parameter	Value at 25°C		Value at 60°C	
	Experimental	Manufacturer	Experimental	Manufacturer
P_{max} (W)	30.93	33.0	26.30	28.2
V_{max} (V)	16.90	16.4	14.0	14.3
I_{max} (A)	1.83	2.01	1.88	1.97
V_{oc}(V)	21.1	21.3	17.9	18.4
I_{sc}(A)	1.95	2.1	2.05	2.14

Intensity, 100 m W cm^{-2}

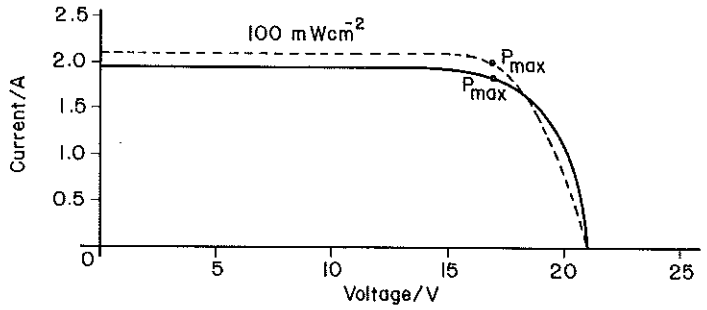

Fig. 16 Comparison of manufacturer's I-V characteristics with those obtained by experiment at 25°C: ––– manufacturer; —— experimental.

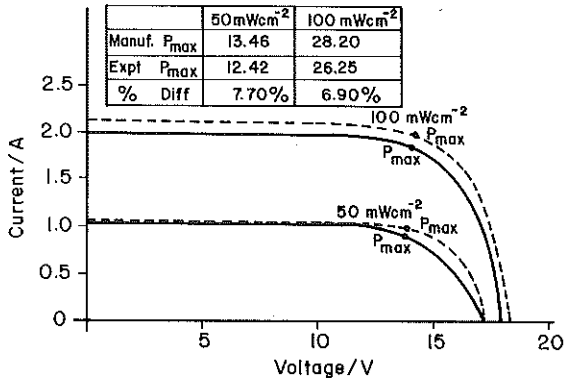

Fig. 17 Comparison of manufacturer's I-V characteristics with those obtained by experiment at 60°C: ––– manufacturer;—— experimental.

Optimum concentration factor for a conventional PV module

The next step was to examine whether the use of the module above a concentration factor of 1 would be possible without a significant decrease in the efficiency.

(a) *Series Resistance Effect*

The curves in Figs. 13-15 could indicate the effect of internal series resistances with increasing irradiance. The short-circuit current was extracted and plotted against the irradiance at 25°C, 45°C and 60°C in Figs. 18, 19 and 20. All three curves (full lines) deviate from the extrapolated straight lines at higher intensities indicating a manifestation of the series resistances. For the curves of 25°C and 45°C the deviation occurs at about 150 mW cm^{-2} and 200 mW cm^{-2} respectively; for 60°C the deviation occurs at 100 mW cm^{-2} [3]. The linearity of the series resistances with the intensity of illumination itself at a particular temperature is apparently governed by the equation

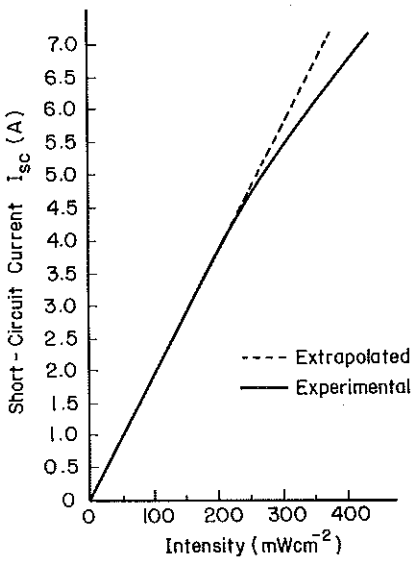

Fig. 18 Short-circuit current vs intensity at 25°C.

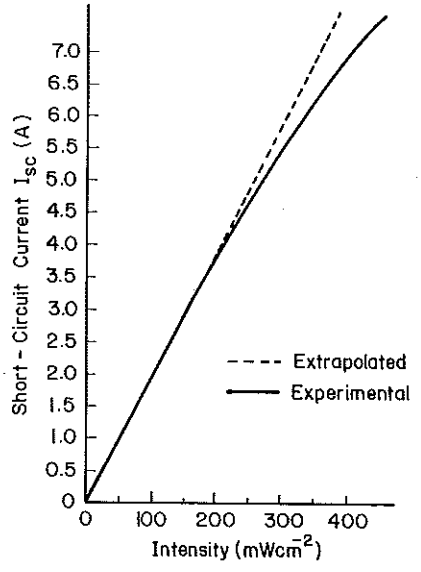

Fig. 19 Short-circuit current vs intensity at 45°C.

$$I_{sc} = I_L - I_o \exp\left(\frac{q\, I_{sc}\, R_s}{AkT}\right) \tag{6}$$

where I_{sc} is the short circuit current (neglecting unity in the usual I-V characteristics equation under illumination) and assuming that $I_{sc}\, R_s$ is negligible. However, for 60°C the linearity deviates at 100 mW cm^{-2} indicating that temperature, in addition to illumination intensity, could cause the series resistance to be effective in the operation of silicon PV modules.

Using equation (6) and the method of Agarwal et al.[4], the plot of $ln\ (I_L - I_{sc})$ versus I_{sc}

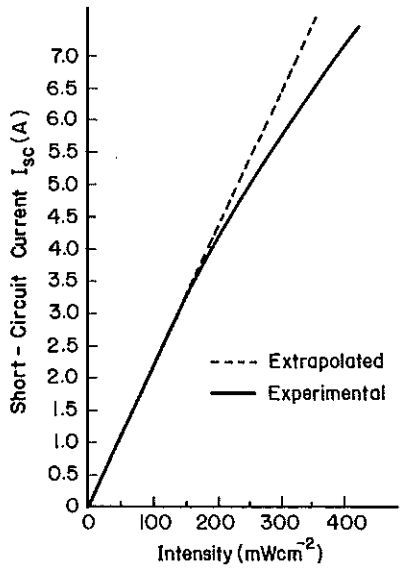

Fig. 20 Short-circuit current vs intensity at 60°C.

should be a straight line. These plots are displayed in Fig. 21, where linearity is exhibited for module temperatures of 25 and 45°C but the curve for 60°C is non-linear. Agarwal et al. considered that non-linearity for such a plot probably occurs when the diode factor A in equation (6) is not a constant.

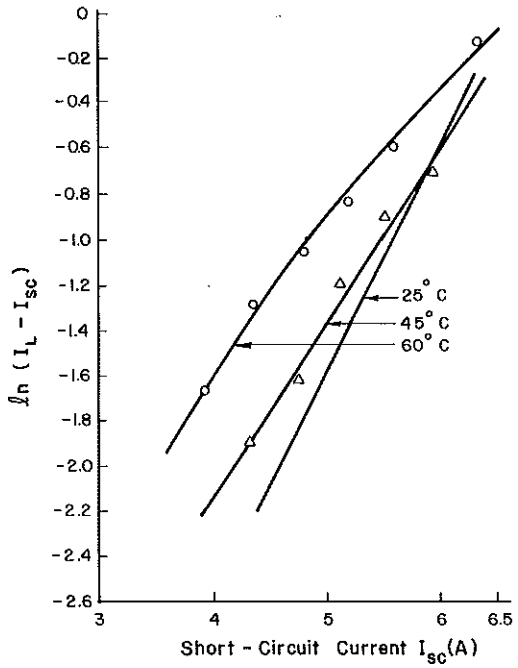

Fig. 21 *ln* $(I_L - I_{sc})$ vs. short-circuit current at various temperatures.

The module parameters were treated in the same way as those of the cells as the difference between them is a glassing factor,

$$F_g = \frac{I_{sc}\ (\text{glassed})}{I_{sc}\ (\text{unglassed})} \tag{7}$$

(b) *Efficiency*

In order to ascertain an optimum concentration factor which lies between 1 and 4 as mentioned earlier, the encapsulated cell efficiencies and module efficiencies were measured for various intensities and temperatures.

The encapsulated cell efficiencies and module efficiencies are plotted against intensity and temperature in Fig. 22. Referring to Fig. 22, at 45°C the module efficiencies at 100 mW cm^{-2} and 200 mW cm^{-2} differ by approximately 0.2%. However, at the same illumination levels, the

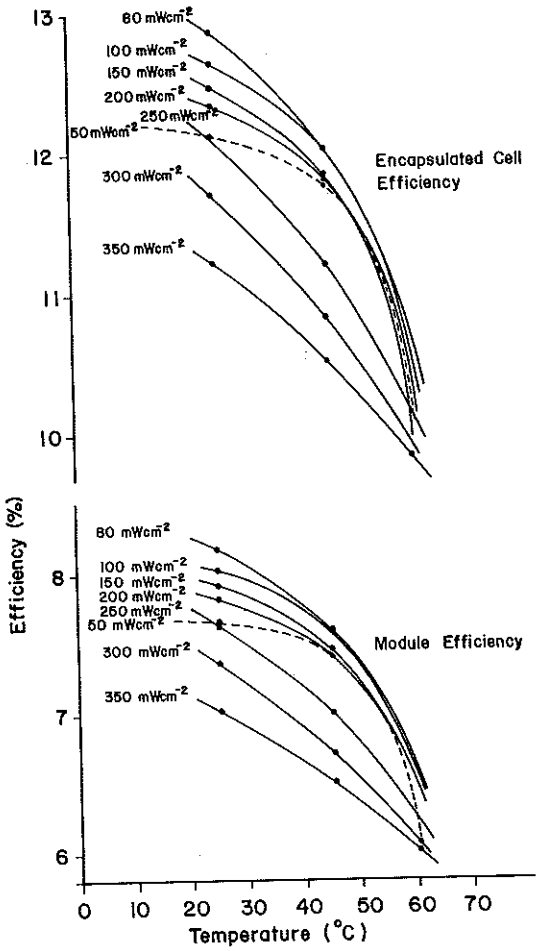

Fig. 22 Efficiency vs temperature.

module efficiency begins to fall quite rapidly from about 7.4% at a temperature of 45°C to less than 6.6% at 60°C as can be seen from Fig. 22. Furthermore, from Fig. 19, the series resistance effect becomes significant about 200 mW cm^{-2}, that is above a concentration factor of two.

These results, thus, indicate that a concentration factor of 2 would be an optimum choice for a conventional PV module operating at 45°C.

Construction of a low concentration PV electric generator with one-axis tracking

After deducing from the measured data the optimum concentration factor of 2 for a conventional PV module, it was duly implemented using a trapezoidal groove of mirrors fitted at an angle of 30° to the normal along the side of the solar modules. This was followed by the sizing of the PV system taking into account the power requirements of the pump-inverter system. A back-up battery was also included in the final set-up to take into account the intermittent availability of solar radiation. Finally, a manual testing of the system was carried out to determine the correct parameters for the implementation of a micro computer system.

Design and construction of trapezoidal groove using mirrors as the concentrator

The low concentration factor of two was achieved by using mirrors of the correct dimensions constructed as shown in Fig. 23.

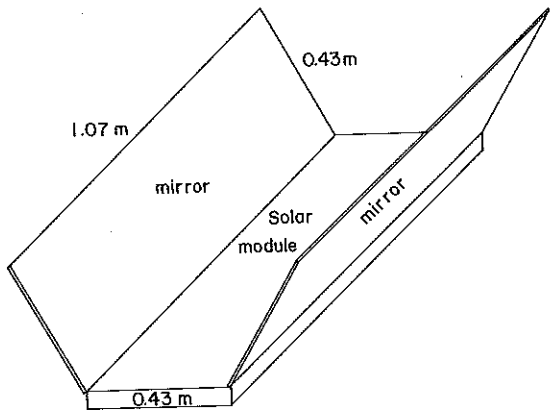

Fig. 23 Low concentrator photovoltaic system using mirrors.

Each PV module was installed with two pieces of mirrors (8 mm thick) of dimensions exactly equal to the dimensions of the module (0.43 m X 1.07 m). The angle of inclination was 30° normal to the plane of the module forming a trapezoidal groove.

For an array system consisting of ten modules, 18 similar equilateral triangular aluminium supports of sides equal to 0.43 m and four right-angled triangular aluminium supports with the length of hypotenuse equal to 0.43 m and base equal to 0.22 m were built and the mirrors were mounted on top of these stands. The two types of aluminium supports are shown in Fig. 24. The dimensions of the aluminium strip used are 0.47 cm X 3.18 cm.

Two different systems of PV modules were built based on the same structural design. One of them is a single row of two TYPE A PV modules connected in parallel without any tracking

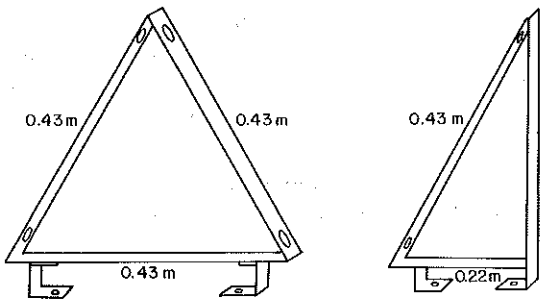

Fig. 24 Aluminium triangular rings for mounting the mirrors.

system and fixed in a horizontal position using dexon angle iron frames. The length of the whole system is in the north-south direction. The other system is made up of ten TYPE B PV modules but arranged in two rows of five modules each placed side by side. This latter system was installed with one-axis mechanically adjustable north-south tracking mechanism.

For the first system, the sun is right over the system only for two short periods in a year, that is, during the 3rd of September and during the 3rd of March of about three days each. Whereas, for the second system, the system can be manually adjusted once every three to five days according to the seasonal position of the sun such that the sun is normal to the panel at noon.

The inverter-pump characteristics

The input/output current and voltage data for the inverter-pump operation is given in Table 3.

Table 3
Input and output current voltage data for the inverter-pump operation.

Input (DC)		Output (AC)		
V	A	V	A	
2.1	0.04	–	–	
4.2	0.095	–	–	
6.4	0.15	–	–	
7.6	15.3	100	0.8	
9.5	19.0	135	0.99	
12.0	21.0	250	1.20	starting
11.0	16.2	186	0.75	operating

The values were plotted in one of the PV modules I-V characteristics curve at 45°C and are shown in Fig. 25. The resultant current-voltage curve is nearly a vertical line in the region of the I-V curve. It shows that the operating point that limits the proportionality of the current to the variation of light intensity is 12 V. For an intensity of 100 mW cm^{-2} the optimum current is 2 A. Therefore, to be able to start the pump at 21 A, the number of modules would be (21/2) = 10.5 modules or to the nearest whole module, 11 modules. Taking into consideration the concentration factor of two, the minimum base requirement of solar radiation intensity is 50 mW cm^{-2}.[5]

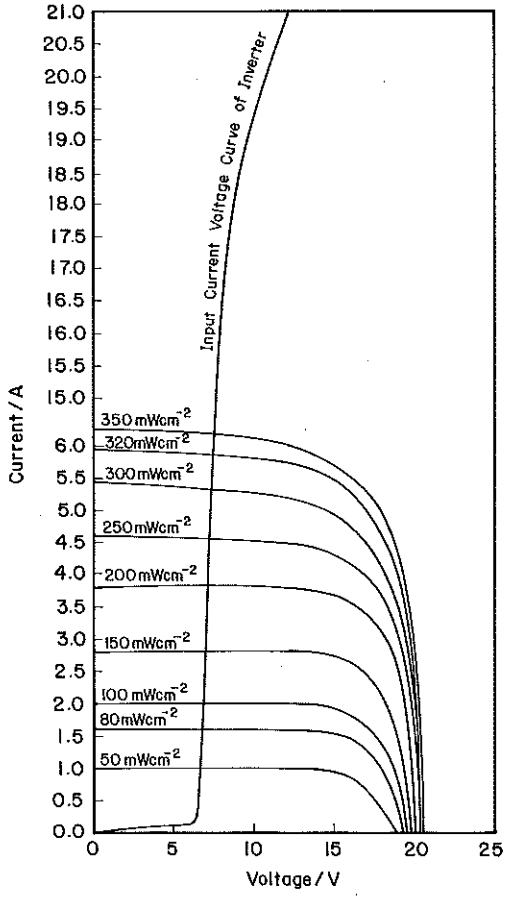

Fig. 25 Current versus voltage at 45°C.

Design of the PV array water pumping system with battery back-up

As can be seen from previous considerations, once the pump is started, the amount of current required to run it continuously is reduced. This means that there will be an excess of current from the PV module if the weather continues to be good.

On the other hand, during adverse weather conditions, or during extreme fluctuation of solar radiation, a back-up battery system has to be incorporated. A circuit was designed such that the

excess current available during good weather conditions can be used to charge an auxilliary storage battery and when the weather is bad another storage battery can be used to run the pump temporarily. This circuit is controlled by means of five relays each of which is opened or closed depending on the condition stipulated. Fig. 26 shows the circuit.

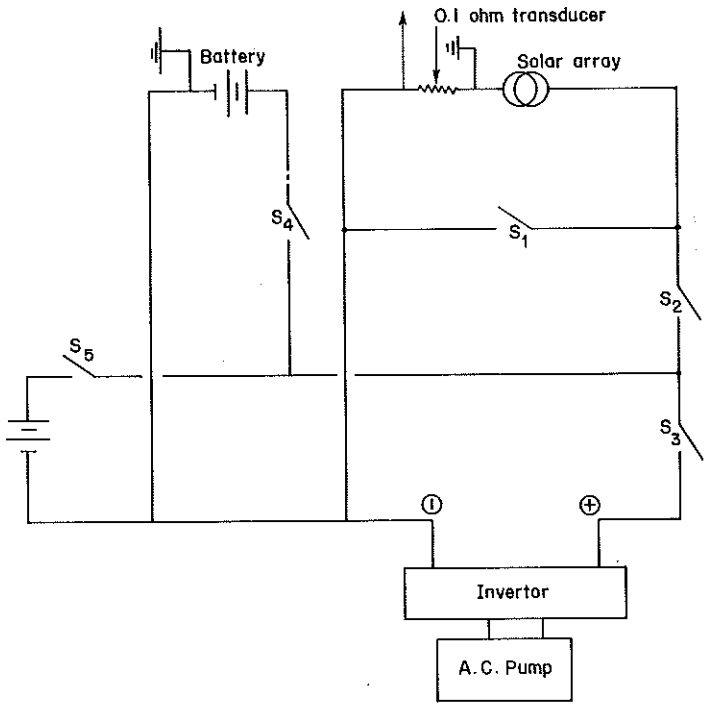

Fig. 26 Relay controlled circuit for PV water pumping system with back-up battery.

The five relay switches, S1, S2, S3, S4 and S5 are either closed or opened depending on the following conditions:

- To start, S1 is closed to determine the short circuit current of the PV modules, I_{sc}.
- If I_{sc} is greater than or equal to the starting current of the pump, i.e., 21A, then S2 and S3 are closed with S1 open.
- If I_{sc} is less than the starting current of the pump and the battery condition is good, the battery is used to start the pump by switching on S2 and S4 with S1 open and then S3 is closed with S4 open; S1 can then be used to check the PV module current again.
- If I_{sc} is less than the starting current of the pump and the battery condition is bad, then S2 and S4 are closed with S1 open. This is to charge the operating battery. A fixed time is given.
- If I_{sc} is sufficient to run the pump and is duly turned on with S2 and S3 closed; any excess current greater than 17A is used to charge an auxilliary battery by closing S5.

The above set-up with manual control was tested using the BPX 47C PV modules and the parameters measured were used in the software design of the microprocessor in Part II.

PART II: DESIGN OF MICROCOMPUTER CONTROL SYSTEM

Introduction

The main function of the microcomputer system is to control the switching of the five mechanical relays to optimise the output of the photovoltaic water pumping system with the back-up battery. Here, optimisation of the output implies the proper management of the energy resources such that the free solar energy is used as far as possible to run the pump with minimum usage of the battery. Precautions are also taken to observe the discharge state of the battery so as to maintain the life-span and also to prevent the battery from being completely discharged.

Before the design and construction of the microcomputer control system, the characteristics of the solar irradiance, including its values and method of measurement, have to be determined so that it can be transduced as an analogue voltage approximately proportional to the actual input value. More important than this is that the voltage has to be converted into digital form using an analogue to digital convertor, since only digital values are acceptable by the microcomputer system.

Next, the condition of the battery has to be determined in such a way that the data can be input into the microcomputer system without affecting the system as a whole, i.e., there should be as little loss in power as possible.

The interrelations between the availability of solar irradiance and the battery characteristics are then studied and managed by the microprocessor which makes use of the software to control the switching relays.

Hardware design and construction

The complete PV solar system using a microprocessor as a control is shown schematically in terms of functional modules in Fig. 27.

Construction of the microcomputer board

Figure 28 shows a block diagram representation of the microcomputer. The central processor unit (CPU) is an INTEL 8085A microprocessor, although other types of microprocessor can accomplish the same function. The INTEL 8085A microprocessor was selected mainly because of the familiarity with the chip and its programming language. Also, because of the availability of the SDK-85 design kit.

The 8085A 8-bit microprocessor with a capacity of addressing up to 64K words of memory and 256 input/output external ports was constructed together with 8755 EPROM and 8155 RAM and a few supporting components. It is operated at 3.072MHz clock frequency using a 6.144MHz crystal. The 8755 provides 2K erasable and reprogrammable read only memory (EPROM) while the 8155 contains 256 bytes of random access memory (RAM). The 8755 also provides 16 input/output (I/O) lines which are programmable as input or output through software control. The 8155 contains 22 I/O lines which are also programmable.

The allocations of the I/O for the various functions are as follows:

i) five output ports from 8755 EPROM are allocated for the five relays;

ii) eight output ports from 8755 EPROM are used to input the digital solar voltage to the microprocessor;

iii) one output port from 8155 chip is used for the start of conversion signal in order to ini-

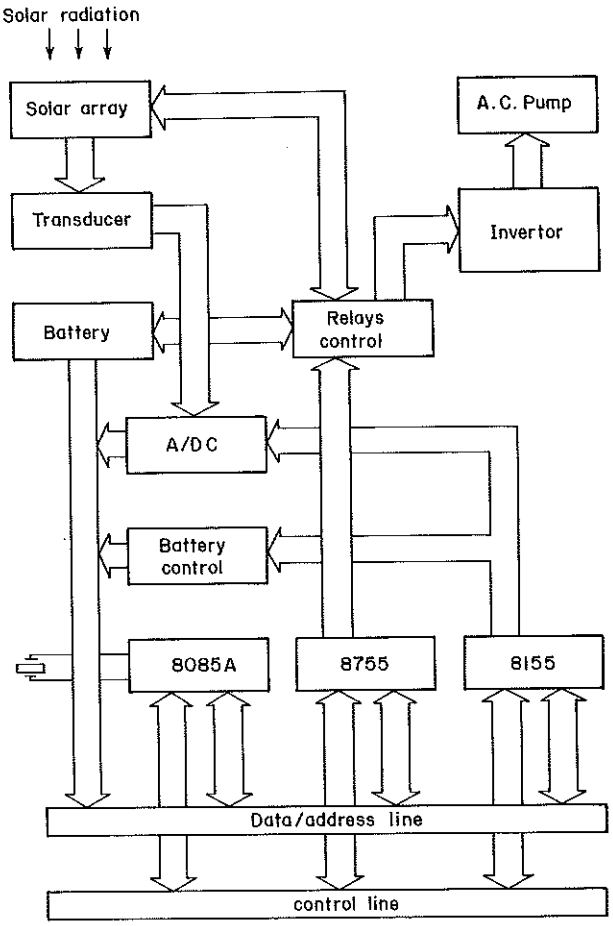

Fig. 27 Schematic representation of the PV waterpump with microprocessor control.

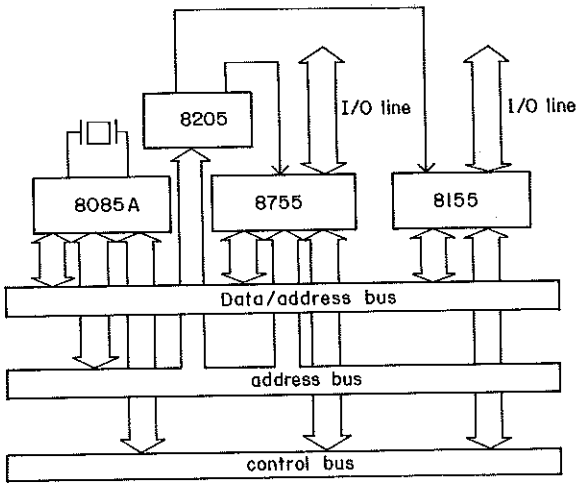

Fig. 28 Block diagram of INTEL 8085A microprocessor based microcomputer.

tiate the analogue to digital conversion; and

iv) two output ports from 8155 chip are allocated for the clock and 'D' signal of a 7474 D-flipflop. The D-flip-flop is to drive an indicator light whenever the battery voltage level falls below a certain number of volts.

Two more output ports from the 8155 chip are used to communicate instantaneously the condition of the battery to the microprocessor. The microcomputer system is assembled according to the above description after it is designed and tested using the SDK-85 kit.

Transducer for the solar radiation

From Table 3, it can be seen that the amount of current generated to operate a 100W (A.C.) pump ranges from 13.5A to 21A after it has been converted into alternating current. It is practically impossible to input this large current into the microcomputer and it has to be transduced into an analogue electric voltage in the range of 1 to 3 volts before being converted into digital form.

The transducer used was simply a high wattage low resistor of 0.1 ohm constructed using ten 1 ohm 30W porcelain resistors connected in parallel. These resistors were placed in an aluminium tray which was fitted with a heat sink to dissipate the heat created. This was to make sure the measured current in terms of voltage was as accurate as possible.

The 0.1 ohm resistor was connected in series with the PV module circuit and the negative terminal was grounded and the voltage at the positive terminal input into the analogue to digital convertor as an analogue voltage, V_{in} as shown in Fig. 26.

Interfacing of analogue to digital convertor to the microcomputer

For the transduced voltage to be digitised, an analogue convertor has to be carefully selected according to the voltage range and the word lengths of the digital output. The RS 8703 8-bit analogue to digital convertor (ADC) was chosen because the voltage input range can be varied easily.

The conversion technique was performed by an increment charge balancing which has inherently high accuracy, linearity and noise immunity. An amplifier integrates the sum of the unknown analogue current and the pulses of a reference current, and the number of pulses needed to maintain the amplifier summing junction near zero was counted. At the end of the conversion, the total count was latched into the digital outputs as an 8-bit binary word. The pin configuration and the absolute maximum rating of the RS 8703 are shown in Fig. 29.

The construction of the ADC circuit, which is shown in Fig. 30 involved the selection of the input resistor, R_{in} and the reference resistor, R_{ref} such that the relations:

$$R_{in} = \frac{V_{in} \text{ full scale}}{10\mu A} \tag{8}$$

and

$$R_{ref} = \frac{V_{ref}}{-20\mu A} \tag{9}$$

where V_{in} full scale is the voltage when the output is at full scale, i.e., the binary word is 11111111.

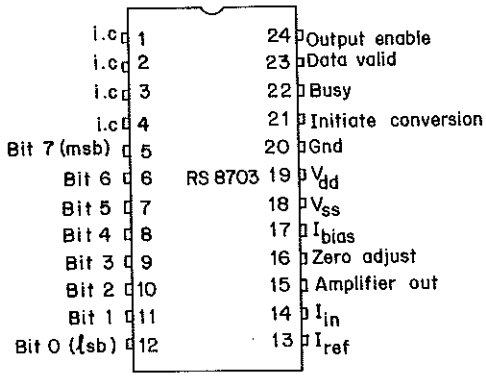

Storage temperature	-65°C to 150°C
Operating temperature range	0°C to 70°C
$V_{dd} - V_{ss}$	18 V
I_{in}	±10mA
I_{ref}	±10mA
Digital input voltage	-0.3 to V_{dd}+.3V
Operating V_{dd} and V_{ss} range	3.5V to 7V
Package dissipation	600 mW
Lead temperature	300°C

Fig. 29 Pin configuration of RS 8703 and its maximum rating.

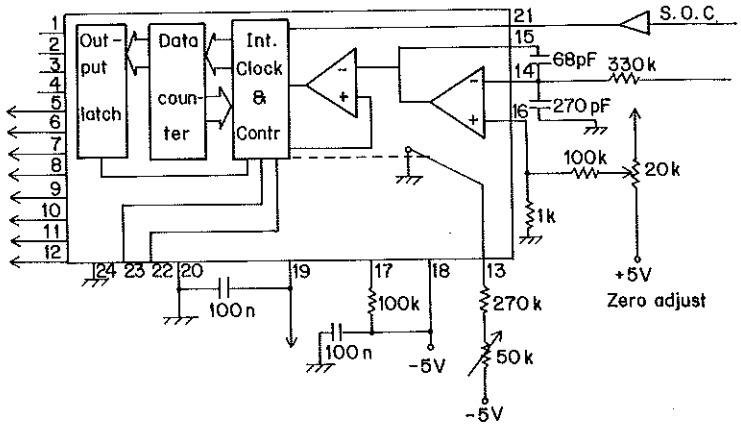

Fig. 30 Analogue to digital conversion circuit.

V_{ref} is the negative reference voltage which is equal to −5V.

were satisfied.

For a transduced voltage of maximum value equal to 3V, V_{in} full scale equals to 3V, thus,

$$R_{in} = \frac{3V}{10\mu A} = 300 \text{ kilo ohm}$$

and

$$R_{ref} = \frac{-5V}{20\mu A} = 250 \text{ kilo ohm}$$

After the ADC was constructed, it was trimmed for zero adjustment by setting the start conversion signal (S.O.C) to a high state and adjusting the zero adjust circuit to obtain a 8-bit word equal, i.e., 00000000 to 00000001 transition and then a full scale adjustment by setting V_{in} to the full scale value less 1½ LSB to trim the gain adjust circuit for a 11111110 to 11111111 transition. The circuit was then tested by varying the voltage and the output pin was observed using LED displays.

Battery control circuit

In a PV system the battery state of charge is of prime importance and the ability to determine it accurately lowers the operating stress of the battery. Various methods have been use to determine the state of a battery.

Here, a low cost battery condition indicator was designed and constructed bearing in mind that the signal obtained can be fed into the microcomputer. The voltage level of 0 to 5 volts acceptable by the microcomputer was also considered.

Figure 31 shows the complete circuit of the battery condition indicator.

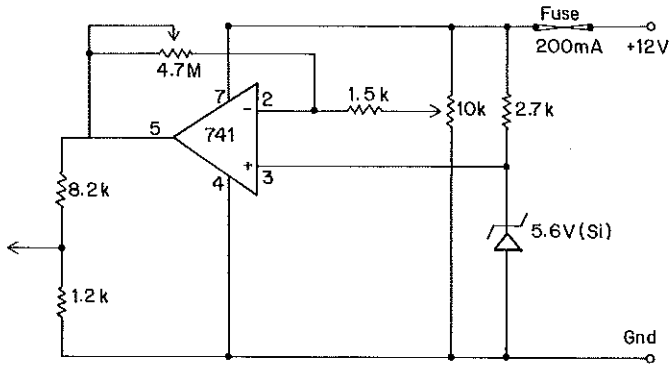

The circuit makes use of a comparator, 741 dual-in-line which compares two divide-by-two voltages of the 12 V battery. One of them is obtained from a 5.6V 400mW silicon Zener diode while the other is from a 2.7 kilo ohm resistor. The former is a relatively stable voltage source of about 6.3 volts while the latter varies depending on the voltage level of the battery. The output

of the comparator is high if the battery state of charge is good. If the state of charge of the battery drops to a certain level which can be set using a variable resistor, the output from the comparator is low. In this circuit, the voltage level which is considered 'bad' is set at 11.5 V and once the state of charge of the battery falls below this a low signal is output.

Design and construction of the relay switching circuit

Governed by the constraints of high direct current, from the solar modules as well as from the battery, five SPST AMF 25A 400mW mechanical relays were used to implement the different combinations of switches in the microcomputer photovoltaic water pumping system. Each relay was protected by a diode connecting across the two terminals. The driver circuit was designed with a 2N 2219 transistor.

Included in the same board were two DPDT 6V 1A mechanical relays, one of which functioned as an automatic switch to control the input power supply while the other one was used to operate an A.C. timer. The first relay was necessary because at any one stage the microcomputer is power-on, all the relays may be turned on resulting in an overloading of the relays which can be easily burned. This relay is controlled by the output of a dual input AND gate (7408) which is in turn controlled by two tri-input NOR gate (7427) with one of the input grounded. The second relay is controlled by the output of a dual input AND gate (7408). The aim of having the timer is to record the duration of water pumping solar energy alone. Fig. 32 shows the TTL circuit for the relays.

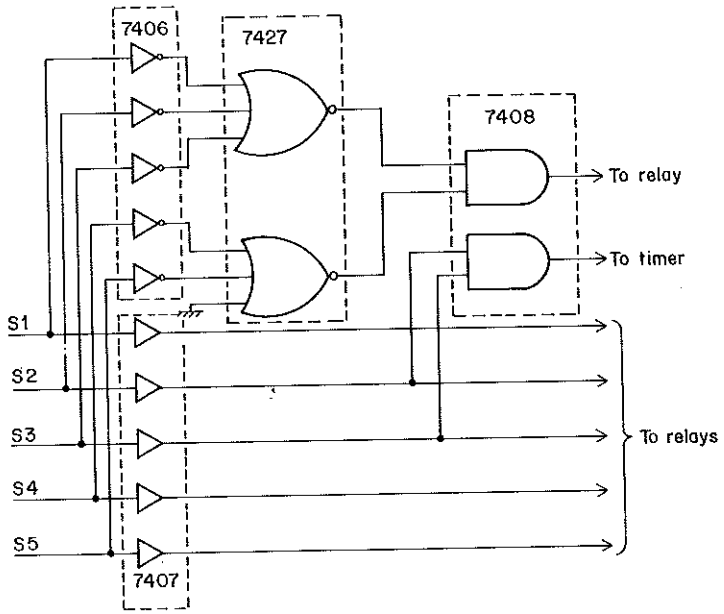

Fig. 32 TTL circuit for the 6V DPDT relays.

The complete circuit diagram set-up of the switching relays is shown in Fig. 33 together with the truth table.

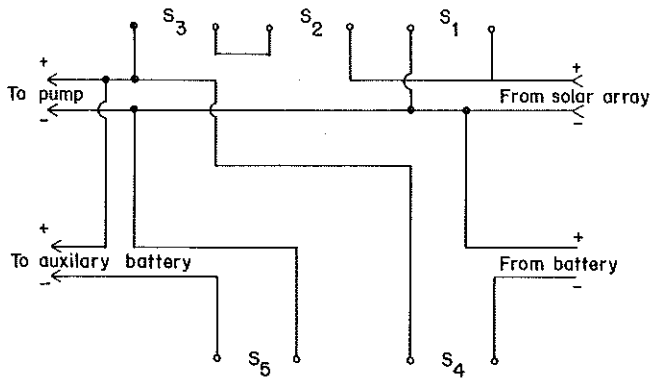

S_1	S_2	S_3	S_4	S_5	Operation
1	0	0	0	0	Measure short-circuit current of array
0	1	1	0	0	Solar array alone operates pump
0	0	0	1	0	Use battery to start pump
0	1	1	0	1	Use extra current to charge auxilary battery
0	1	1	1	0	Battery and solar array operate pump and in process of switching over
0	1	1	0	1	Charging of auxilary battery using excess current

Fig. 33 Relays switching circuit and the truth table.

Testing the functionality of individual printed circuit boards

The complete hardware set-up consisting of five printed circuit boards, viz, SDK-85 board, the ADC board, the battery condition indicator board, the relay switching control board and the power supply board, was installed in an aluminium chassis. Before installation, these five microprocessor control system components were tested individually for continuity, shorts and its functionality. The analogue to digital convertor was tested using analogue voltage supply from a power supply and controlled by a variable resistor. The output signal was tested by connecting the eight outputs to eight LED display panels. Varying the voltage between the 3V range gave different combinations of '1' and '0'. The output value was counter-checked using the theoretical calculated values. Table 4 shows the set of the digital values in hexadecimal code of analogue voltage from 0V to 2.5V.

The battery condition indicator circuit was tested by setting the preset and varying the input voltage from 12 V to the set voltage, also using a variable power supply. The output was checked using a LED display. A high output lights up the LED while a low output does not.

The relay switching circuit board was tested by supplying a "1" state or a "0" state signal to individual relay and its functionality observed.

Table 4
Digital values (in hexadecimal) of analogue voltage from 0V to 2.5V

Analogue voltage (V)	Digital value (Hexadecimal)
0.00	00
0.10	00
0.20	08
0.30	12
0.40	1D
0.50	27
0.60	31
0.70	3B
0.80	44
0.90	4E
1.00	59
1.10	63
1.20	6C
1.30	77
1.40	81
1.50	8A
1.60	95
1.70	9E
1.80	A8
1.90	B2
2.00	BD
2.10	C8
2.20	D2
2.30	DA
2.40	E4
2.50	EE

Software design details

The software development proceeded concurrently with the hardware design and construction. The problems encountered during the software development may well call for substantial hardware modifications like the inclusion of a relay for the power supply and the timer to record the number of hours of pumping using purely solar energy. Extra precautions were taken particularly in the condition for any input/output parameters to be activated; for example, the initialization of a '1' state to the start of conversion (SOC) signal to the ADC in order to start the analogue conversion and the sending of a clock signal in order to set a D-flip-flop after the 'D' signal is in a '1' state. The software development is divided into three distinct phases which are described in the following three sub-sections:

The production of flow charts

In this stage of the software development, a logical sequential flow of the program is drawn bearing in mind the aim of making maximum use of available solar radiation to pump water with maximum usage of back-up battery system and if necessary, using the excess available solar energy

to charge the battery. Based on the parameters identified in the section "Design of the PV array water pumping system with battery back up" of Part I, a flow chart can be constructed and is shown in Fig. 34.

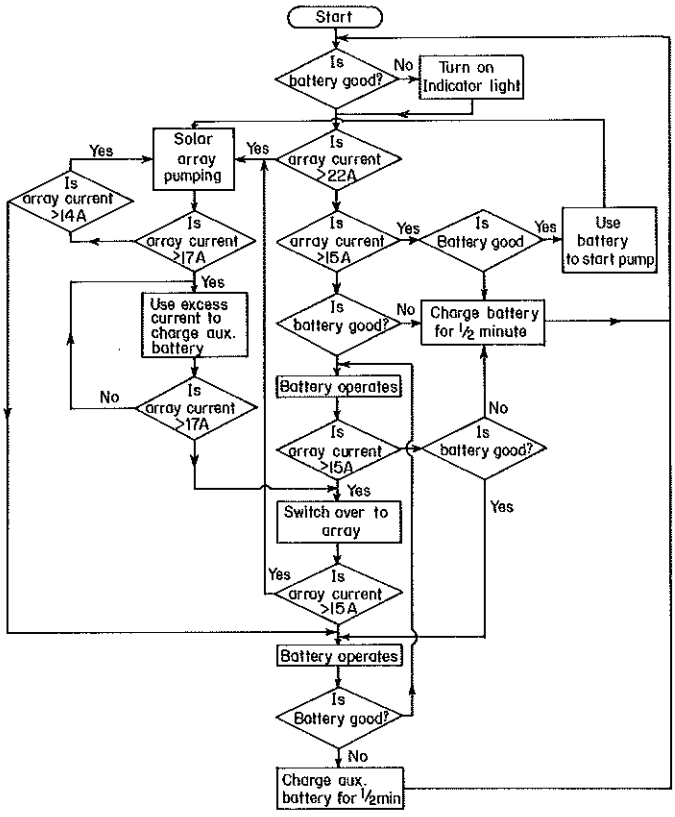

Fig. 34 Flow chart for PV water pumping using microprocessor control system.

The program starts with the initialization of the I/O ports in order to input and output the signals to and from the microcomputer. Once this is done, the microcomputer inputs the battery condition indicator signal and turns on an indicator light if the battery is considered in bad condition. If the battery condition is good, the array current is next checked.

If the array current is greater than 22A, the pump operates using only solar energy. Then, the microcomputer continues to check whether the array current is greater than 17A during operating mode. If it is greater than 17A, the excess current is drawn to charge a battery. If it is less than 17A but greater than 14A, the pump continues to operate using solar energy. But, if it is less than 14A, the battery is used to operate the pump.

During pump operation using the battery, the microcomputer keeps checking the array current so as to switch over to the solar array once the condition is met.

If the array current is less than 22A but greater than the operating current of the pump, and

the battery is in good condition, the battery is used to start off the pump and switch over to the solar array after a few seconds. If at any time, the battery is discharged and the solar energy is insufficient to operate the pump, it is used to charge the battery for 30 seconds and the whole routine starts all over again.

The translation of flow chart into 8085 machine code

The assembly language program was keyed into INTEL MDS microcomputer development system and compiled. This compiled program is in object code which is then converted into hexadecimal code. The program in hexadecimal code is in fact a machine code acceptable by the microcomputer. These different versions of the program were all stored in an eight inch double-density diskette to facilitate documentation and future program modification.

Testing of the program

The testing of the software is in fact the testing of the whole microcomputer system including the hardware. Before the testing could be done, the microcomputer board was substituted using an INTEL SDK-85 design kit since a special test driving program can be entered using hexadecimal code into the 8155 RAM through the keyboard. The keyboard is controlled by the 8279 keyboard controller. The testing of the software was done piece-wise, i.e. individual hardware and software modules were tested to determine whether the I/O behaviour conformed to design specification. The ADC software was tested together with the relays switching circuit using the start of the conversion subroutine. The flow chart is shown in Fig. 35.

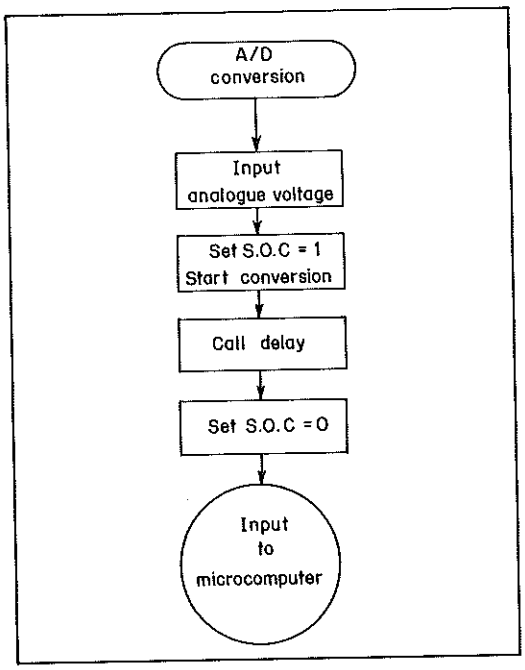

Fig. 35 Flow chart for SOC sub-routine.

The ADC test program is

```
MVI   A, 81H     ; close S1
OUT   00         ; input voltage
CALL  DELAY      ; 1 millisecond delay
MVI   A, 01H     ; set SOC = 1
OUT   21H        ; start conversion
NOP
NOP
NOP
LXI   D, 0FFFH   ; set-up delay
CALL  DELAY      ; call delay sub-routine
MVI   A, 00      ; set SOC = 0
OUT   21H        ;
IN    01H        ; input to microcomputer
MOV   C, A       ; store in register C
HALT
```

This same program was executed using different input analogue voltage and the converted digital output was displayed. The program was also in a way testing the I/O port assignment initialisation and the relay control board.

Next, the battery condition indicator together with the indicator light were tested and the flow chart is as shown in Fig. 36.

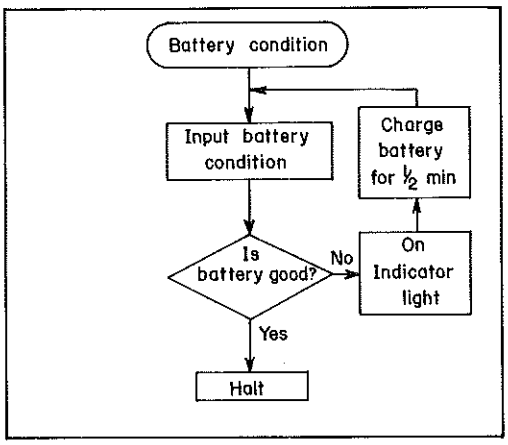

Fig. 36 Flow chart for battery condition indicator testing.

The test program for the battery condition indicator circuit is

```
BATT:   IN     22H      ; input battery voltage
        CPI    08H      ; is battery good?
        JC     CHARGE   ; jump if bad
        HALT
```

```
CHARGE: MVI   A, 41H     ; set D = 1 state in D-flip-flop
        OUT   21H
        NOP
        NOP
        NOP
        MVI   A, C1H     ; set clock = 1 state in D-flip-flop
        OUT   21H
        NOP
        NOP
        NOP
        MVI   A, 41H     ; reset clock = 0
        OUT   21H
        MVI   A, 25H     ; switch on S3 and S6
        OUT   00         ; to charge battery
        LXI   D, 8000H   ; 30s delay
        CALL  DELAY
        JMP   BATT
```

After these two testings, a stage is reached where all the component modules were linked together into a whole system which again was tested on its functionality to verify its input/output behaviour. This time, the complete program was keyed into the 8155 RAM but tested in an 'artificial' and controllable environment. That is, the battery input and the solar irradiance input were substituted using variable power supply. Different combinations of voltages within real time situations were applied and the I/O behaviour was observed and necessary modifications in either hardware or software were made.

Performance testing of microcomputer control system

The final phase of testing placed the system with the complete and wholly integrated hardware and software components in its working environment connected to the transducer, the battery, the solar arrays, the invertor and the AC pump, as shown in Fig. 37.

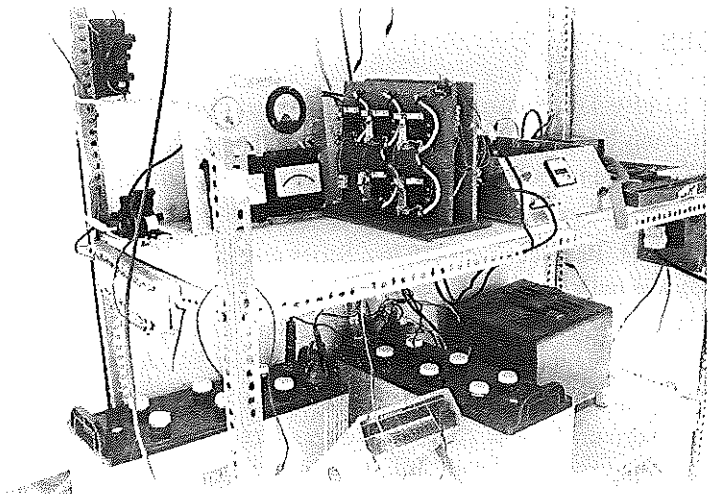

Fig. 37 PV water pumping using microprocessor control.

In this final test, the program was not stored in the 8155 RAM as it was earlier, but was burned in the 8755 EPROM. The burning process was done in INTEL TECHNOLOGY SDN BHD in Bayan Lepas using the Universal PROM Programmer Model UPP-103. Special attention was focussed on the following:

a) The proportionality of the input solar current and the digital output from the ADC. This is to ensure that the heat dissipated at the transducer does not affect the accuracy of the measurement. To check this, an ammeter is connected in series with the input solar current before passing through 0.1 ohm transducer and counter-check with the combinations of the relays which are turned on according to the specifications in the program.

b) The sensitivity of the microcomputer in making a decision whenever there are any changes in the condition. Here, close observation on the speed of changing over to another combination of relays closed when the weather condition changes has to be done over a considerable period to increase confidence.

c) The continuity of the water pumping process is closely observed whenever there is a change of combinations of relays. This is to make sure no additional energy is wasted when the pump has already been started and, more important, to achieve the aim of maximum pumping rate.

d) The productivity of the whole system is also considered. Here the rate of the flow of water at which it is considered significant during pumping using solar energy is observed. This is not significant if only two gallons of water are obtained in ten minutes using solar energy but is on the other hand, if we get 20 gallons of water using battery to operate the pump over the same period. This is the reason why from the earlier study, the pump can operate at about 13A and yet in the program, 15A is the criteria for the microcomputer to decide whether to use the battery or the solar array to operate the pump.

e) The reliability of the system as a whole is taken care of by running the operation for a considerable length of time. Here, the breakdown period is recorded and the kind of problems encountered are also recorded.

REFERENCES

1. Teoh, C.L. (1984), *Photovoltaic solar system with microprocessor control,* M.Sc. thesis, Universiti Sains Malaysia, Penang.

2. Teoh, C.L., Donald G.S. Chuah, S.L. Lee and G.S. Rao (1983), An optimum concentration factor for conventional silicon photovoltaic modules, *Solar Cells,* Vol. 10, pp. 223-236.

3. Wolf, M. and H. Rauschenbach (1976), Series resistance effects on solar cell measurements, In C.E. Backus (ed), *Solar Cells,* IEEE, New York, p. 146.

4. Agarwal, S.K., R. Muralidharan, A. Agarwala, V.K. Tewary and S.C. Jain (1981), A new method for the measurement of series resistance of solar cells, *J. Physics D,* 1981, p. 1643.

5. Teoh, C.L., Donald G.S. Chuah, S.L. Lee and G.S. Rao (1982), An experience with photovoltaic modules under low concentration and an AC pump, *Proceedings of US-ASEAN Seminar on Energy Technology,* LIPI, Bandung, Indonesia, 7-18 June 1982, pp. 366-385.